Near-wall turbulence structure in the plane turbulent wall jet in still surroundings

by

J.G. Eriksson and R.I. Karlsson

Vattenfall Utveckling AB

SE-814 26 Älvkarleby, Sweden

(Also the Faxén Laboratory, Royal Institute of Technology, S-100 44 Stockholm, Sweden)

ABSTRACT

Three-component laser-Doppler velocimetry measurements have been performed in a plane turbulent wall jet. Through the use of light collection in 90° side-scatter together with optics such that the probe volumes have small diameters, detailed measurements could be performed down to $y^+ \sim 1.8$. Turbulence statistics up to fourth order moments are reported for all three velocity components. In order to obtain correct measurements in the near-wall region, an adequate data refinement procedure is essential. This includes the criteria for removal of "bad samples" as well as correcting for small non-orthogonalities in the experimental set-up. When the turbulence statistics of the wall jet is compared to that of the flat plate boundary layer, a qualitatively very similar behaviour is seen. On the other hand, quantitative differences are observed in some of the higher order moments, especially in the viscous sub-layer.

1. INTRODUCTION

A wall jet may be defined as "a shear flow directed along a wall where, by virtue of the initially supplied momentum, at any station, the streamwise velocity over some region within the shear flow exceeds that in the external stream" (Launder and Rodi, 1981). Wall jets are of great engineering importance with many applications. Some examples are defrosters in automobiles where wall jets are used for mass transfer modifications, and aero engines and stationary gas turbines, where wall jets are used for cooling of combustion chamber walls and the leading stages of the turbine itself.

The turbulent wall jet is also a basic flow of fundamental interest because of its two-scale character. The inner layer of the plane wall jet is similar to that of the turbulent boundary layer, while the outer layer resembles that of a free (plane) jet. The interaction of large turbulence scales in the outer layer with smaller scales in the inner layer creates a complicated flow field and determines the development of the wall jet. The flow situation is sketched in figure 1, which also gives the relevant nomenclature.

The literature on wall jets is immense. Launder and Rodi (1981, 1983) reviewed the experimental literature up to 1980. Reviews of the more recent literature are found in eg. Abrahamsson et al. (1994) and George et al. (2000). Recent major experimental studies of turbulent wall jets are the work by Wygnanski et al. (1992) and Abrahamsson et al. (1994) who used HWA to study the wall jet in stagnant surroundings, and the work by Schneider (Schneider (1987), Schneider and Goldstein (1994)) and Eriksson et al. (1998), who used LDV. A recent theoretical work is that by George et al. (2000),

This not withstanding, there are still unknowns in relation to the plane wall jet, particularly concerning the inner layer. The previous work by Eriksson et al. (1998) covered a comparatively long interval in streamwise position, x/b = 5 to x/b = 200, but was restricted to two velocity components. It was therefore decided to supplement that data set with three component measurements with high spatial resolution, taken at a few streamwise positions in the developed region of the flow. Consequently, a repeat of the wall jet experiment has been performed (Eriksson, 2000). In the present report, we will focus on higher order turbulence statistics in the near-wall region. Following a short presentation of the test facility and the instrumentation, the optical set-up and the experimental methodology is described. The data refinement procedures are given in some detail. Turbulence data up to fourth order moments is presented. Whenever possible, the turbulence statistics of the wall jet is compared to the statistics of the flat plate boundary layer.

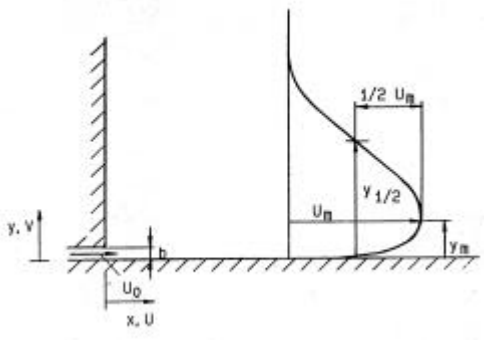

Figure 1. Configuration and nomenclature for the plane wall jet.

2. EXPERIMENTAL APPARATUS AND PROCEDURE

2.1 Wall jet test facility

The original test facility is shown in figure 2. It consists of a large tank into which a jet discharges. The tank is 7 m long and its width is 1.45 m. One of the side walls is made of glass, as well as the bottom. A large contraction (Morel, 1975) with a turbulence-reducing screen inserted is used to produce a fairly flat mean velocity profile at the inlet. A weir upstream of the contraction keeps the upstream water level constant, and the flow velocity through the slot is set by an adjustable weir at the downstream end at the tank. Taking the mean slot height to 9.6 mm and using water of room temperature, an inlet velocity of 1 m/s results in a nominal inlet Re-number (Re_0) of approximately 9600. For a more detailed description, refer to Eriksson et al. (1998).

In order to achieve optical access for the measuring of the spanwise velocity component, the test section had to be modified. Originally, the space between the bottom of the test section and the bottom of the tank was water-filled to decrease the load on the test section glass bottom. A large, slightly oval ”box”, open at its top and bottom, was now fitted into this space and sealed against the surrounding water. Thus a dry space was created immediately under the test section, in which a fiberoptic probe with traversing equipment could be placed. (Refer also to figure 3 showing a sketch of the final experimental set-up.)

The size and position of the box was restricted both by the positions of the load-bearing beams under the water tank and those under the glass bottom. The length of the box was 1540 mm, starting at x=180 mm. Its width was 348 mm, starting at z=275 mm. To get the maximum variation of the measurement position, this number has to be decreased by two times the probe radius (probe diameter is 83 mm). This left us with a principle maximum variation of 265 mm, centered at z=449 mm. Consequently, it was not possible to make spanwise velocity measurements on the centerline.

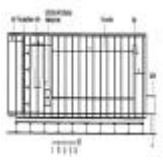

Figure 2. Wall jet test facility

2.2 Instrumentation

The LDV hardware consisted of a TSI Colorburst for frequency shifting and colour separation, six fiberoptic couplers, two TSI 2-component fiberoptic probes, a TSI Colorlink including receiving optics and frequency mixing electronics, and a 3-component TSI IFA750 signal processor. The fiberoptic probe used to measure the streamwise and normal velocities was mounted on a three-axis traverse table and equipped with an extra 2.6x beam expander. An upper-central beam arrangement was used to measure the normal velocity component, see Karlsson & Johansson (1988). A front lens with a focal distance of 450 mm was used, which was enough to reach the spanwise positions where 3-component measurements were possible, while still giving small probe volumes. The resulting optical probe volume dimensions, based on the e^{-2} intensity cut-off point, were (0.37 × 0.038) mm (streamwise velocity component - 488 nm) and (0.78 × 0.040) mm (normal velocity component - 514.5 nm), respectively. The probe used to measure the spanwise component was mounted on a one-axis traverse system, and had no extra beam expansion. The front lens focal distance was 250 mm, resulting in a (0.74 × 0.054) mm measuring volume (476 nm). The relevant optical parameters are summarized in table 1.

Standard TSI software (FIND version 4.5) running on a 486 PC was used for data collection and all initial data reduction except higher order mixed moments (for which extra software had to be written). Silicon carbide particles with a mean diameter of 1.5 μm were used to seed the flow.

Table 1. Optical parameters at x/b = 70

	Normal velocity	**Streamwise velocity**	**Spanwise velocity**
? (nm)	514.5	488	476
d_{pv} (μm)	40	38	54
l_{pv} (mm)	0.78	0.37	0.74
Fringe distance (μm)	3.76	1.80	2.48

2.3 Optical set-up

A three-component measurement with high spatial resolution is obtained through a combination of light collection in 90° side-scatter and the use of optics such that the probe volumes have small diameters. For the optics used, the receiving volume diameter is about twice the measuring volume diameter, meaning that the lengths of the measuring volumes are reduced to approximately two times the diameter of the measuring volume (probe volume) of the receiving probe.[1]

[1] Apart from improving the spatial resolution, this also minimizes possible effects of fringe distortion due to improper beam crossing.

A cross-section of the test rig and the experimental set-up, with the 476 nm probe under the bottom of the tank, is shown in figure 3. The (almost) horizontal probe 1 is used to measure the normal and streamwise velocities. The light scattered from the two probe volumes is collected through the vertical probe 2. Probe 2 emits the violet beams used to measure the spanwise velocity, and the scattered light from this probe volume is collected through probe 1. The length of the effective probe volume used to determine the spanwise component is thus determined by probe 1, and is approximately 0.08 mm normal to the wall. Direct backscatter light collection is avoided, which improves the signal-to-noise ratio for all velocity components close to the wall.

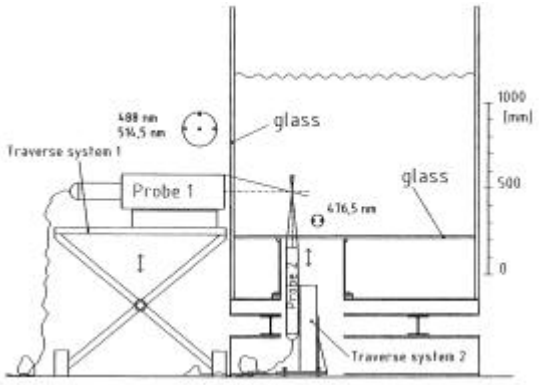

Figure 3. Experimental set-up for three-component measurements

2.4 Experimental methodology

Initially, a number of Pitot tube measurements were made at different spanwise positions at the slot, x = 0, to check inlet conditions. As in the previous wall jet study (Eriksson et al., 1998), very flat velocity profiles were found. No spanwise variations in the maximum slot velocity were seen.

LDV-measurements were taken at the streamwise positions x/b = 70, 100 and 150. During the x/b = 70 - main series, measurements were made both as two- + one-component measurements and as simultaneous three-component measurements. (Two- + one-component meaning that the spanwise component measurements at a point were separated in time from the streamwise and normal component measurements.) Furthermore, all two-component measurements were taken in two different signal processor modes, one allowing multiple measurements per burst (MMPB)[2], and one allowing only one measurement to be made on every burst (SMB). Whenever the latter mode was used, the particle residence times were also recorded.

The vertical profiles of the main measurement series were taken in the order given above. The difference in height between the upstream and downstream free surfaces, $?h$, and the water temperature, $T_{0,}$ were checked regularly during each measurements series, in order to detect any drift in inlet velocity or inlet Re-number.

All measurement series started at the wall, y = 0. A preliminary wall position was determined by observing the output signals (blue and green channels) from the processor, i. e. after amplifying and filtering, on an oscilloscope. The ”wall signal” is very characteristic. The distance from the preliminary wall position was then measured by a dial gauge. (The corresponding preliminary wall distance was adjusted after the measurements, see section 3.1.) As far as possible, traversing was made upwards only, to avoid hysteresis in the measurement of the traversing distance. During the very near-wall measurements, probe 1 was traversed while probe 2 was kept fixed. Thus the blue and green mv:s move along the violet mv. The use of side-scatter light collection means that the wall distance for the spanwise component measurements is determined by the vertical position of the receiving volume of probe 1.

Samples were taken for a constant time at each measuring point, instead of taking a constant number of samples. This avoids the problems with independent samples, since soon as the data rate is larger than ~ 1 sample per integral time scale, the number of integral time scales rather than the number of samples determines the statistical

[2] George (personal communication) has pointed out the equivalence of this technique to residence time weighting, since the velocity of each particle is effectively ”weighted” by the length of time it is present in volume.

uncertainty (Buchhave et al., 1979). Sampling times of 15, 20 and 25 minutes respectively were used at the three streamwise positions. Slightly shorter times were used for the very near-wall measurements.

Shift frequencies were chosen such that all likely flow angles were measured with equal probability (Whiffen 1975; Buchhave 1975, 1979), while still staying away from the filter limits. When performing multi-component measurements, it was tried to choose a coincidence window long enough to avoid sorting out low velocity particles while still short enough to avoid combinations of bursts emanating from different particles.

3. DATA TREATMENT

3.1 Determination of wall distance and wall shear stress

Near the wall, the momentum equation for the plane wall jet can be approximated as

$$0=\frac{\partial}{\partial y}\left(-\overline{uv}+n\frac{\partial U}{\partial y}\right) \tag{3.1}$$

Integrating, evaluating the constant of integration at y = 0 and switching to wall variables, we obtain

$$\overline{uv}^{+}=\frac{\partial U^{+}}{\partial y^{+}}-1 \tag{3.2}$$

If the appropriate near-wall series expansions for U^+ and uv^+, see e.g. Launder (1984), are inserted in the eq. (3.2), it follows immediately that the second non-zero term in the series expansion for U^+ must be of fourth order in y^+. I.e.

$$U^{+}=y^{+}+C_4 y^{+^4}+\cdots \tag{3.3}$$

Or in terms of an unknown wall position y_0

$$U^{+}=(y^{+}-y_0^{+})+C_4(y^{+}-y_0^{+})^4+\cdots \tag{3.4}$$

The wall shear stress and the wall distance was determined by fitting the experimental data to eq. (3.4), with u^*, y_0 and C_4 as free parameters.[3] Practically, the fitting process was made in two steps. First with three free parameters. Based on this a best estimate of y_0 was made. The fitting was then repeated with a fixed wall distance. This procedure was used to minimize the scatter in u^*. (Fits with three free parameters using a corrected wall distance repeatedly gave $y_0 < 0.001$ mm.)

The primary advantage of the inclusion of the fourth order term is that it increases the region of convergence of the expansion. Using data from a larger interval in y^+ decreases the sensitivity of the fit to single erroneous data points. Figure 4 gives an example of a near-wall velocity distribution and the corresponding curve fit. The position of the first data point corresponds to $y^+ = 1.4$, the position of the last data point to $y^+ = 6.1$. Over this interval, the removal (or inclusion) of single data points changed the estimated value of u^* by less than ± 0.3%, as long as a sufficient number of data points were used. [4]

[3] All curve fitting was made in KaleidaGraph™, using a non-linear least squares method.

[4] For this specific measurement series, a wall distance correction of 0.028 mm was applied. The estimated y_0 after this correction was ~0.0003 mm.

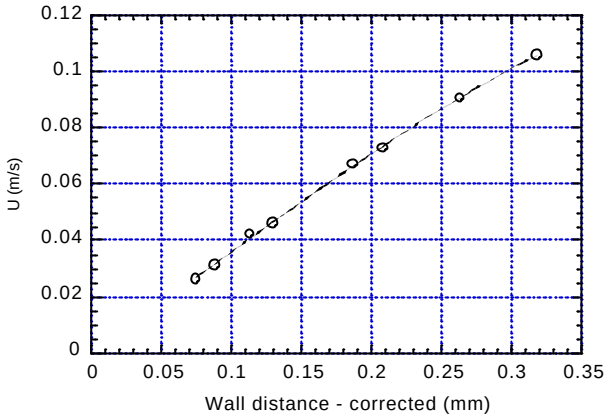

Figure 4. Example of near-wall velocity distribution used for determination of u^*

3.2 Data refinement

3.2.1 Corrections for non-orthogonalities

Karlsson et al. (1993) gave a detailed discussion of the consequences of a small deviation from orthogonality between the measured streamwise and normal components, and derived relevant corrections for V, v´ and $\overline{uv}$. They also verified the corrections experimentally. Defining the deviation angle (correction angle, angle error) α positive in the clockwise direction and assuming the streamwise component to be accurately aligned (index "o" refers to quantities in an orthogonal system; index "m" to quantities actually measured), the corresponding corrections for the higher order moments are as follows:

$$\left(\overline{u^2 v}\right)_o = \frac{1}{\cos a}\left[\left(\overline{u^2 v}\right)_m - \overline{u_o^2}\sin a\right] \tag{3.5}$$

$$\left(\overline{uv^2}\right)_o = \frac{1}{\cos^2 a}\left[\left(\overline{uv^2}\right)_m - \sin 2a\left(\overline{u^2 v}\right)_o - \overline{u_o^3}\sin^2 a\right] \tag{3.6}$$

$$\overline{v_o^3} = \frac{1}{\cos^3 a}\left\{\overline{v_m^3} - 1.5\sin 2a\left[\left(\overline{uv^2}\right)_o \cos a + \left(\overline{u^2 v}\right)_o \sin a\right] - \overline{u_o^3}\sin^3 a\right\} \tag{3.7}$$

$$\overline{v_o^4} = \frac{1}{\cos^4 a}\left[\overline{v_m^4} - \overline{u_o^4}\sin^4 a - 4\sin^3 a\cos a\left(\overline{u^3 v}\right)_o - 6\sin^2 a\cos^2 a\left(\overline{u^2 v^2}\right)_o - 4\sin a\cos^3 a\left(\overline{uv^3}\right)_o\right] \tag{3.8}$$

The methodology used to determine the deviation angle a is given in detail in Karlsson et al. (1993). We may expect a more accurate determination for the present experiment, since measurements could be taken closer to the wall.

Naturally, a corresponding set of equations can be used to correct for the non-orthogonality that is inherent in the arrangement used for making measurements close to the wall. Due to the combination of a slightly tilted LDV-system and the use of an upper-central beam configuration, the measured vertical component will always be tilted relative to the normal of the wall. The equations will not be shown, since they can be obtained from the original set simply by replacing *u* with *w* and utilizing the fact that a number of flow variables can be assumed to equal zero due to two-dimensionality. (Eg. *W*, $\overline{uw}$, $\overline{w^3}$ and $\overline{u^2 w}$)

3.2.2 Bad samples

When trying to compute higher order moments, the removal of "bad samples" from a data set is particularly important. Johansson (1988) classified the bad samples in "outliers" and "sharp peaks". He also showed, for a flat plate boundary layer (FPBL), that the influence of the sharp peaks usually were negligible compared to that of the outliers. Consequently, we will concentrate on the latter.

An outlier may be defined as a sample that falls severely outside the central part of the probability density function (PDF). An often used method to eliminate such samples is based on the assumption that all samples falling outside an interval "mean value ± ?s" are to be considered as bad. The final statistical values are then computed on the truncated data set. This method has the advantage that it can be performed automatically. It is, on the other hand, almost impossible to decide beforehand a proper choice for ?. (Furthermore, if the PDF:s are skew, different values for ? should be used at the upper and lower end.) It will often lead to the removal of good samples, which introduces an error by itself. This has been very clearly illustrated by Xu et al. (1996), who computed the near-wall kurtosis of the normal velocity fluctuations (F_v) for their DNS-results on pipe flow. A strong effect was seen when the velocity fluctuations above a certain number of rms-values were omitted, even with ? as high as 10.

The method that has been used here is that by Johansson (1988). In principle, it is based on the assumption that the PDF, or the number density function (NDF) should be continuos. If the entire velocity interval between the minimum and the maximum values is divided into a fixed number of intervals, say 100, and the number density function plotted, an outlier is defined as a single sample having a significant number, say 10, of empty intervals between itself and the next sample. (A detailed description of the algorithm is found in Johansson (1988)) If the number of samples per unit time is high enough so that the velocity signal is virtually continuos, it is possible to judge the "badness" of the sample by visual inspection of the velocity traces. This is not the case for the present investigation, so all prospective bad samples have been considered bad and consequently been removed.

An illustration of the typical effect of the removal of outliers is given in table 2. The measurements were taken at y^+ ~ 3.1. 4 samples of originally 23352 were removed. The effects on the streamwise velocity quantities were negligible (less than the experimental uncertainty), so those results are not shown.

Table 2. Illustration of the effects of removal of outliers.

	V (m/s)	**v´(m/s)**	**S_v**	**F_v**	**uv $(m/s)^2$**	**u^2v $(m/s)^3$**	**uv^2 $(m/s)^3$**
Raw data	0.0002813	0.003342	-0.442	19.1	-3.55e-5	-3.76e-6	4.68e-7
Outliers removed	0.0002840	0.003303	-0.287	15.1	-3.45e-5	-3.53e-6	4.28e-7

3.3.3 Further near-wall corrections

The variance $\overline{u^2}$ used to compute the turbulent kinetic energy (k) has been corrected for gradient broadening. Corrections have not been applied to S_u and F_u, since Durst et al. (1992) have shown them to be rather insensitive to gradient broadening. The variance $\overline{v^2}$ has been corrected for system noise according to Eriksson et al. (1999)

4. RESULTS

All wall jet data presented here were taken at the streamwise position x/b=70, i.e. at a streamwise position where the flow has been shown to be fully developed while yet not influenced by the return flow (Eriksson et al., 1998). A summary of fundamental flow quantities is given in table 3. Furthermore, all data presented were taken as two + one component measurements. No simultaneous three-component data will be presented, since these measurements are still being analyzed.

Table 3. Compilation of fundamental flow quantities at x/b = 70. Repeated wall jet experiment.

	WJ
U_0 (m/s)	1.083
u^* (m/s)	0.02432
U_{max} (m/s)	0.410
C_f	0.00703
$y_{1/2}$ (mm)	55.6
y_{max} (mm)	8

l^+ (µm)	40.59
? (m^2/s)	$0.987 \cdot 10^{-6}$

To the best of the authors' knowledge, inner layer data on the third and fourth order moments for the wall jet have not been available earlier. We will therefore make certain comparisons to FPBL-data. When the source is not explicitly stated, the data of Karlsson & Johansson (1988) and Johansson & Karlsson (1990) has been used.

Figure 5 illustrates the influence of collecting scattered light in 90° off-axis as compared to direct backscatter. The normal turbulence intensity is plotted versus wall distance. Inner scaling is used. WJ91 refers to the earlier experiment by Eriksson et al. (1998), whereas WJ95 refers to the repeated wall jet experiment. It is obvious that data could be obtained closer to the wall. It is also obvious that there is a lot less noise in the data below $y^+ = 4$.

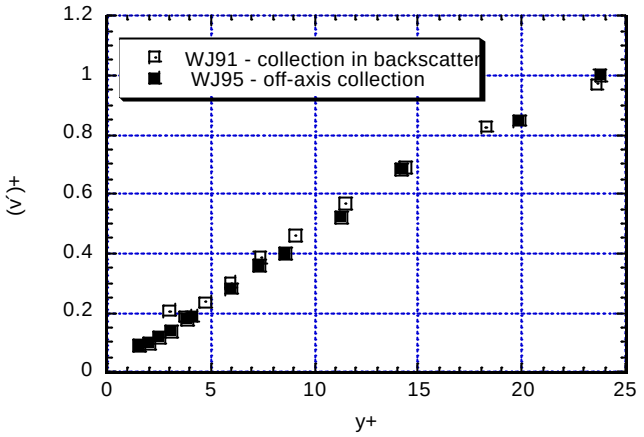

Figure 5. Normal turbulence intensity in inner scaling.

Figure 6a) shows the turbulent kinetic energy, $k \equiv \frac{1}{2}\overline{u_i u_i}$, in inner scaling. A preliminary k‡- profile was published in Eriksson et al. (1999). The profile shown here is thought to be more accurate, since the data refinement is completed. A few new points have been added in the very near-wall region. There is now clearly a tendency towards an inner peak located at $y^+ \sim 20$, i.e. close to the position of the $(u')^+$-peak. In terms of k^+, this inner peak has a value of about 8.5. An slightly decreasing k^+ is seen over the interval $20 = y^+ = 200$, followed by a strong outer peak, $k^+ \sim 15$, located at $y^+ \sim 1100$. Not surprisingly, the position where k^+ starts to increase again corresponds well with the position of the mean velocity maximum, ?U/?y = 0. Using outer variables, the position of the outer peak corresponds to $y/y_{1/2} \sim 0.8$. Also shown, as a solid line, is the first term in the near-wall expansion $k^+ = 0.5\left(a_u^2 + a_w^2\right)y^{+2}$, where a_u and a_w are the leading terms in the series expansions of the streamwise and spanwise velocity fluctuations. a_u and a_w has been taken as 0.45 and 0.27, respectively (Eriksson et al. 1999).

Figure 6b) compares the k-distribution of the wall jet to that of the FPBL. The profiles are qualitatively quite similar, but the actual levels are about twice as high for the wall jet (WJ).

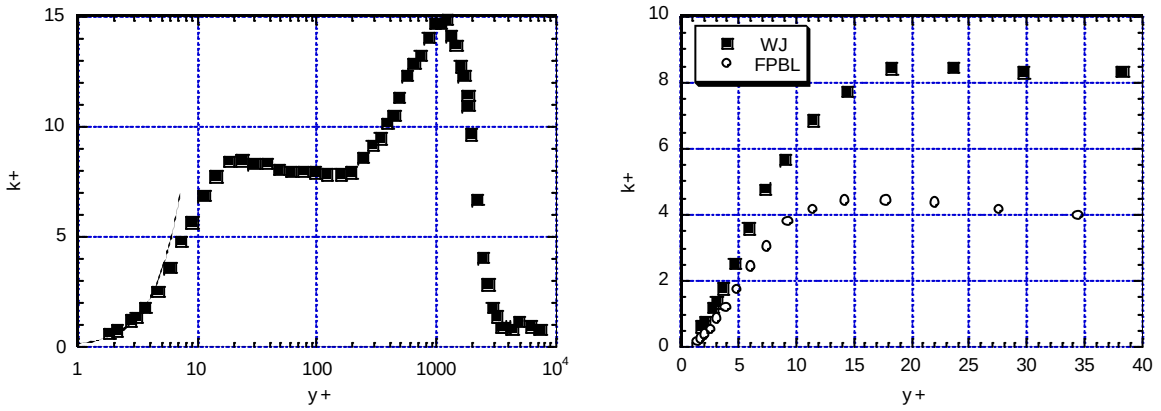

a) *b)*

Figure 6. Turbulent kinetic energy of the WJ in inner scaling. a) Entire profile. b) Comparison to FPBL in the near-wall region.

Figure 7 shows the distributions of the skewness of the streamwise (S_u) and the normal (S_v) velocity fluctuations in the wall jet and in the FPBL, respectively.[5] We may again note that the profiles are qualitatively very similar. There are, however, quantitative differences, especially in S_u for which the FPBL-values are consistently lower than the WJ-values. The zero-crossing takes place at $y^+ \sim 25$, as compared to $y^+ \sim 14$ for the FPBL. The maximum value, appearing in the viscous sub-layer, is ~ 0.9 for the FPBL versus ~ 1.3 for the WJ. (It can be noted that according to the literature review by Fernholz & Finley (1996), peak values of S_u in the FPBL from 0.9 to 1.65 have been reported.) A range of negative values of S_v is seen for both data sets, from $y^+ \sim 20$ for the WJ and from $y^+ \sim 30$ for the FPBL. There is a certain amount of scatter in the data, but the minima in S_v appears to be at $y^+ \sim 4$ for both flowfields, the actual level being slightly more negative for the WJ. For both data sets, S_v is slightly positive inside $y^+ \sim 2$.

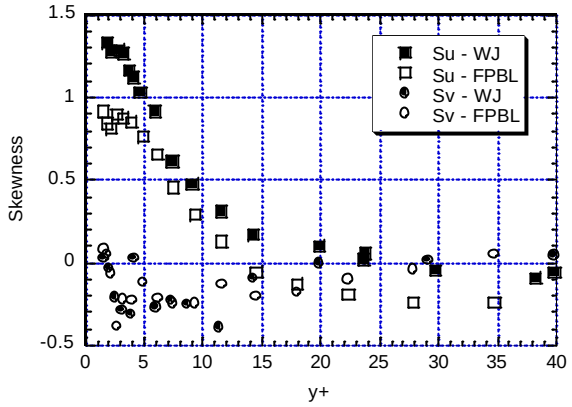

Figure 7. Skewness factors near the wall.

Figure 8 presents the flatness for the streamwise and spanwise components, F_u and F_w. The general behaviour is once again much in line with that of the boundary layer. There is a very small difference in F_u outside $y^+ \sim 5$, the WJ-levels being only slightly larger. On the other hand, when the viscous sub-layer is approached, the curves diverges quite strongly. The maxima is ~ 4 for the FPBL and ~ 6.5 for the WJ. As opposed to F_u, F_w does not go to a value < 3 in the range shown in figure 8. Rather, it increases continuously from $y^+ \sim 40$ and inwards, consequently being significantly larger than F_u from $y^+ \sim 20$ to $y^+ \sim 5$. Its maxima is approximately equal to that of F_u, ~ 6.5. FPBL – data on F_w in the viscous sub-layer have not been available for comparison.

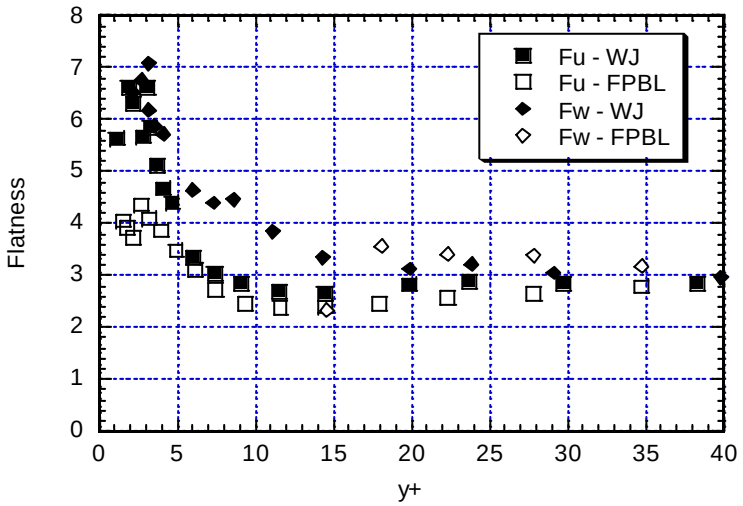

[5] The skewness of the spanwise velocity fluctuations, S_w, was approximately constant, $S_w \sim 0.1$, through the y^+-range shown in figure 7. We have to interpret that as a weak three-dimensional effect.

Figure 8. Flatness factors near the wall.

In figure 9, experimentally determined flatness factors F_v for the WJ and the FPBL are shown together with DNS-results for pipe flow (Xu et al., 1995). Yet again, we see a very good agreement between the WJ and the FPBL except very near the wall, here $y^+ = 10$, where the WJ shows considerably higher values. The maximum value is almost twice as high for the WJ, ~ 15 vs ~ 8 for the FPBL. The maximum is found at $y^+ \sim 3 - 5$, which is slightly further out from the wall than the corresponding maxima of F_u and F_w. A significant difference between the experiments and the simulation results is seen for very small y^+. When the wall is approached, the experimental data reaches a maximum whereafter it decreases, while the simulation results show a steep rise all the way to $y^+ = 0$. Xu et al. (1996), using results from DNS as well as from experiments, argued that this is indeed a real physical effect, caused by very strong events appearing only in the near-wall region and being rare in time as well as space. We have presently no explanation as to why this behaviour is not seen in our experimental results. We can, however, speculate that it is related to the presence of noise in the measurements. The fact that F_v from the WJ91-experiment (not shown here) is considerably lower than F_v from the WJ95-experiment in the region where the latter provided "more noise-free" v´-measurements (refer to fig. 5), hints in that direction.

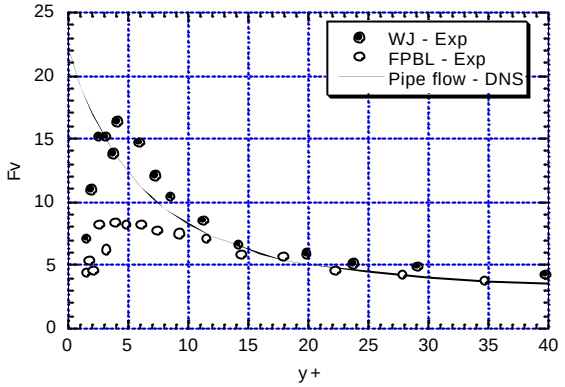

Figure 9. The near-wall kurtosis of v.

Figure 10 shows the correlation coefficient uv/u´v´ (C_{uv}) vs y^+. The shear stress itself, in inner scaling, is almost identical for the WJ and the FPBL for $y^+ < 40$ (George et al., 2000). Since both u´ and v´, in inner scaling, is larger for the WJ, the correlation coefficient must have a smaller value in the same region. C_{uv} is obviously very sensitive no noise in the normal component. When $y^+ \to 0$, C_{uv} should go towards a finite value equal to $(a_{uv}/a_u \cdot a_v)$, where a_{uv}, a_u and a_v are the leading terms in the corresponding near-wall series expansions. It is very difficult to get a good experimental determination of a_v, since it requires noise-free measurements very close to the wall. Using the estimates given in Eriksson et al. (1998), a value of -0.13 is obtained for C_{uv}. Applying the same kind of estimates on the new data, $C_{uv} \sim -0.2$ is obtained. The latter value is expected to be more adequate, due to the improved near-wall data.

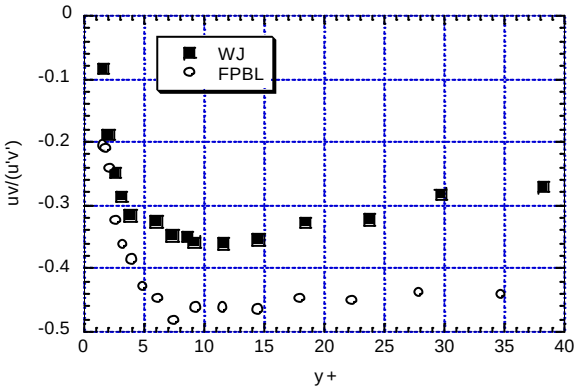

Figure 10. Correlation coefficients near the wall.

Figure 11 shows the mixed third order moments $(u^2v)^+$ and $(uv^2)^+$. $(u^2v)^+$ starts out by going negative, with a minima of ~ -0.8 at $y^+ \sim 7$. A zero-crossing occurs at $y^+ \sim 15$, and a maxima of ~ 1.2 is seen at $y^+ \sim 50$. $(uv^2)^+$ starts

positive, with a maxima of ~ 0.2 at y^+ ~ 12. The zero-crossing occurs at y^+ ~ 25-30. At y^+ = 50, $(uv^2)^+$ ~ -0.4. Further out, it decreases continuously out to y^+ ~ 500. As compared to the FPBL-data, the inner peaks in both $(u^2v)^+$ and $(uv^2)^+$ are stronger, but occurs at the same positions as in the boundary layer. The zero-crossing for $(uv^2)^+$ occurs further out for the WJ, as does the positive peak in $(u^2v)^+$.

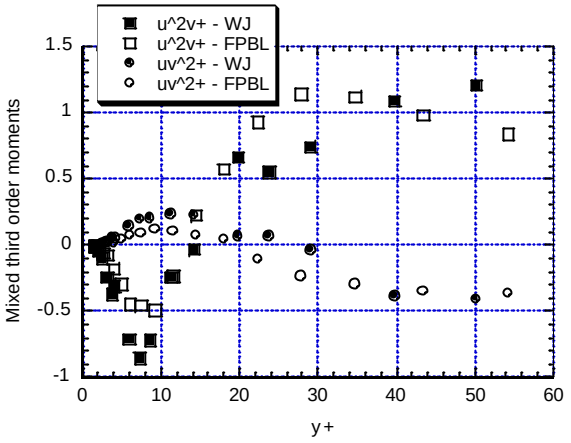

Figure 11. Mixed third order moments in inner scaling.

5. CONCLUSIONS

Detailed three-component turbulence measurements in a wall jet down to $y^+ < 2$ have been accomplished through a combination of light collection in 90° side-scatter and the use of optics such that the probe volumes have small diameters. A complete k-profile has been obtained, and turbulence statistics up to fourth order have been presented for all three velocity components. Comparing the wall jet to the flat plate boundary layer, one finds that the turbulence structure in the near-wall region is qualitatively very similar but that the actual values of the quantities (in conventional inner scaling) consequently are higher in the wall jet. A similar behaviour was observed for the second order moments by Eriksson et al. (1998).

REFERENCES

Abrahamsson H; Johansson B; Löfdahl L (1994) A turbulent plane two-dimensional wall jet in a quiescent surrounding. European Journal of Mechanics B. Fluids 13: 533-556

Buchhave P (1979) The measurement of turbulence with the burst-type laser doppler anemometer – errors and correction methods. Ph.D. Thesis, State University of New York at Buffalo

Buchhave P (1975) Biasing errors in individual particle measurements with the LDA-counter signal processor. Proceedings of the LDA-Symposium Copenhagen 1975, Dantec Measurement Technology, Skovlunde, Denmark

Buchhave P; George WK; Lumley JL (1979) The Measurement of Turbulence with the Laser Doppler Anemometer. Ann. Rev. Fluid Mech. 11: 443-503

Durst F; Martinuzzi R; Sender J; Thevenin D (1992) LDA-measurements of mean velocity, rms.values and higher order moments of turbulence intensity fluctuations in flow fields with strong velocity gradients. Sixth Int Symp on Applications of Laser Techniques to Fluid Mechanics. Lisbon, Portugal.

Eriksson J; (2000) The 1995 Wall Jet Experiment. Part 1: Methodology, Data Treatment and Selected Results. Internal report UI 00:02, Vattenfall Utveckling AB.

Eriksson J; Karlsson R; Persson J (1999) Some new results for the turbulent wall jet, with focus on the near-wall region. Proc. 8th Int. Conf. on Laser Anemometry – Advances and Applications. University of Rome "La Sapienza", Rome, Italy.

Eriksson J; Karlsson R; Persson J (1998) An Experimental Study of a Two-Dimensional Plane Turbulent Wall Jet. Exp Fluids 25: 50-60

Fernholz HH; Finley PJ; (1996) The incompressible zero-pressure-gradient turbulent boundary layer: an assessment of the data. Prog. Aerospace Sci. 32: 245-311

George WK; Abrahamsson H; Eriksson J; Karlsson R; Löfdahl L; Wosnik M (2000) A Similarity Theory for the Turbulent Wall Jet Without External Stream. Submitted to Journal of Fluid Mechanics

Johansson G (1988) An experimental study of a flat plate turbulent boundary layer, using laser-Doppler Velocimetry. Ph D Thesis, Chalmers University of Technology, Göteborg, Sweden

Johansson TG; Karlsson RI (1989) The Energy Budget in the Near-Wall Region of a Turbulent Boundary Layer. Applications of Laser Anemometry to Fluid Mechanics, Eds. R.J. Adrian et al. Springer-Verlag Berlin Heidelberg, pp. 3-22.

Karlsson R; Eriksson J; Persson J (1993) LDV Measurements in a Plane Wall Jet in a Large Enclosure. Laser Techniques and Applications in Fluid Mechanics, Eds. R.J. Adrian et al., Springer Verlag, Berlin-Heidelberg.

Karlsson R; Johansson G (1988) LDV measurements of higher order moments of velocity fluctuations in a turbulent boundary layer. Laser Anemometry in Fluid Mechanics III, Eds. RJ Adrian et al., Ladoan – Instituto Superior Technico, Lisbon.

Launder BE (1984) Second-moment closure: methodology and practice. In Turbulence models and their applications. Vol 2. Editions Eyrolles, Paris, France.

Launder, BE; Rodi, W (1983) The Turbulent Wall Jet - Measurements and Modelling. Ann. Rev. Fluid Mech. pp. 429-459.

Launder BE; Rodi W (1981) The turbulent wall jet. Prog Aerospace Sci 19: 81-128

Morel T; (1975) Comprehensive Design of Axisymmetric Wind Tunnel Contractions. J. Fluids Eng. 977: 225-233.

Schneider ME (1987) Laser Doppler measurements of turbulence in a two-dimensional wall jet on a flat plate in stagnant surroundings. Ph.D. Thesis, University of Minnesota

Schneider ME; Goldstein RJ (1994) Laser Doppler measurement of turbulence parameters in a two-dimensional plane wall jet. Phys. Fluids, Vol. 6, pp. 3116-3129

Whiffen MC (1975) Polar response of an LV measurement volume. Minnesota Symposium on Laser Anemometry, University of Minnesota, Minneapolis

Wygnanski I; Katz Y; Horev E (1992) On the Applicability of Various Scaling Laws to the Turbulent Wall Jet. J. Fluid Mech., Vol. 234, pp. 669-690.

Xu C; Zhang Z; den Toonder JMJ; Nieuwstadt FTM (1995) Origin of high kurtosis levels in the viscous sublayer. Direct numerical simulation and experiment. Phys. Fluids 8: 1938-1944